machines

MDPI

Article

Geometric Accuracy Design and Tolerance Allocation of Precision Horizontal Machining Centers

Lina Wang [1,2], Xingxing Liu [2], Wenjie Tian [3,*] and Dawei Zhang [2]

[1] School of Mechanical Engineering, Tianjin Sino-German University of Applied Sciences, Tianjin 300050, China; wanglina@tsguas.edu.cn
[2] Key Laboratory of Mechanism Theory and Equipment Design of Ministry of Education, Tianjin University, Tianjin 300072, China; liuxxtju1215@163.com (X.L.); medzhang@tju.edu.cn (D.Z.)
[3] School of Marine Science and Technology, Tianjin University, Tianjin 300072, China
* Correspondence: wenjietian@tju.edu.cn

Abstract: As the structural complexity of machined components increases and the pace of product updates accelerates, the demands for machining precision in CNC machine tools are becoming increasingly rigorous. Consequently, the continuous enhancement of machining accuracy in machine tools presents a significant challenge that must be addressed within the realms of machine tool innovation and the development of manufacturing equipment. This paper conducts a comprehensive investigation into the tolerance optimization allocation method for geometric accuracy in precision horizontal machining centers utilizing interval theory. Initially, a mapping model is developed to represent each source of geometric error and the overall spatial error, drawing upon multi-body system theory. Subsequently, the global maximum interval sensitivity of each geometric error source in relation to the overall spatial model is analyzed. Finally, an interval optimization model for geometric accuracy is formulated based on interval optimization theory, employing a genetic algorithm to address the accuracy allocation problem associated with various error sources in machine tools.

Keywords: precision horizontal machining center; interval theory; geometric error modeling; interval sensitivity analysis; optimal allocation of geometric accuracy

Academic Editor: Kai Cheng

Received: 31 January 2025
Revised: 19 February 2025
Accepted: 24 February 2025
Published: 26 February 2025

Citation: Wang, L.; Liu, X.; Tian, W.; Zhang, D. Geometric Accuracy Design and Tolerance Allocation of Precision Horizontal Machining Centers. *Machines* **2025**, *13*, 187. https://doi.org/10.3390/machines13030187

1. Introduction

Accuracy serves as a critical metric for evaluating the performance of CNC machine tools, as it is intrinsically linked to product quality, production timelines, manufacturing costs, and overall market competitiveness [1]. As the complexity of machined parts increases and product innovations accelerate, the demands for machining accuracy in machine tools have become increasingly stringent [2]. Consequently, the continuous enhancement of machining accuracy presents a significant challenge that must be addressed to foster advancements in machine tool technology and the broader equipment manufacturing sector.

Several factors influence the accuracy of machine tools, including geometric errors, thermal errors, assembly errors, cutting-related errors, and errors associated with fixtures. Notably, geometric errors contribute to approximately 20–30% of the total error in machine tools. Therefore, it is imperative to conduct geometric accuracy design prior to the manufacturing and assembly processes to effectively enhance the spatial accuracy of the entire machine [3–5]. Geometric accuracy design encompasses two primary components: geometric accuracy analysis and geometric accuracy allocation. The former involves estimating the spatial error of the entire machine based on the known geometric errors of individual components utilizing a spatial error model [6]. The latter, geometric accuracy allocation,

entails determining the geometric error for each component through a precision reverse model or a precision optimization distribution model, thus falling under the category of reverse precision design [7,8].

Research on geometric accuracy design is typically structured around three key steps: geometric error modeling [9–11], geometric sensitivity analysis [12–14], and geometric error distribution [15]. In the realm of error modeling, the geometric error modeling approach grounded in multi-body system theory has garnered significant attention [16]. This theory allows for the abstraction of mechanical systems and effectively characterizes their motion properties, rendering it a robust and efficient modeling technique. The geometric error modeling method based on multi-body system theory consolidates structural errors and kinematic pair errors into motion transformation matrices and structural transformation matrices, respectively. It integrates various error components, including geometric, thermal, and load-related errors, into the structural and motion error terms, thereby establishing a comprehensive expression for the spatial error of machine tools. This methodology is characterized by its broad applicability, systematic specification, and straightforward derivation process, enabling rapid modeling through computer programming, albeit with limitations in computational efficiency.

The contemporary landscape of geometric error sensitivity analysis is primarily concerned with various analytical methods for assessing sensitivity, including traditional approaches such as the difference method, perturbation method, and matrix differential method. A notable challenge associated with the difference and perturbation methods is the determination of an appropriate step size, which can lead to a substantial increase in the workload required for sensitivity calculations. In a study conducted by Chen et al. [17], the local sensitivity analysis method was employed to investigate the sensitivity of 37 error sources related to spatial errors in five-axis ultra-precision machine tools, with the findings subsequently applied to the design and manufacturing processes of these machines [18]. Additionally, an interval analysis method for parameter sensitivity was utilized to analyze the sensitivity of a plane strain structural foundation model, resulting in the derivation of a sensitivity factor matrix for eight parameters of the Duncan–Chang model [19]. Ye et al. [20] examined the sensitivity of manufacturing and assembly errors in relation to machine tool spatial errors using the difference method, identifying key manufacturing errors that influence machine tool spatial errors, thereby providing a theoretical foundation for the accuracy distribution of machine tools. The matrix differential method can impose specific requirements on the form of the sensitivity solution [21]. However, in cases where the response function is discontinuous or non-differentiable, achieving a sensitivity solution using the aforementioned methods can be problematic. From a statistical perspective, researchers have proposed a sensitivity analysis method based on the Monte Carlo approach to address error modeling. Nonetheless, the Monte Carlo method entails significant computational demands, particularly when applied to implicit limit state equations [22]. Although the use of importance sampling can mitigate computational burdens, it is not well suited for addressing small-probability problems. In contrast, sensitivity analysis methods grounded in interval theory offer a viable solution to the limitations of traditional sensitivity calculation techniques, particularly in the context of nonlinear systems, where they demonstrate enhanced computational efficiency and accuracy in results.

For precision machine tools, the sensitivity of different geometric error sources to the overall spatial error of the machine tool exhibits variability. Concurrently, the degree of control over these geometric error sources during the manufacturing and assembly processes also differs [23]. In actual manufacturing and assembly processes, the magnitude of each error source is often not a fixed number but rather an interval with associated errors [24]. Using a tolerance optimization allocation method that assumes equal precision

or equal impact can inevitably lead to tolerances of geometric errors being either too large or too small in practical design and manufacturing [25–27]. Excessively high precision can result in unnecessary cost waste, while excessively low precision may fail to meet the design requirements for the overall spatial accuracy of the machine [28].

This article studies the optimization allocation method for the geometric accuracy of precision horizontal machining centers based on interval theory. First, a mapping model between various geometric error sources and the overall spatial error of the machine is established based on multi-body system theory. Then, the interval sensitivity of each geometric error source to the overall spatial error of the machine is analyzed across the entire working space. Finally, an optimization allocation method for manufacturing tolerances of components based on interval optimization algorithms is proposed, and a genetic algorithm is used to solve for the tolerance bands corresponding to each error source of the machine tool.

2. Geometric Error Modeling

Geometric error modeling is a prerequisite for optimizing the allocation of geometric accuracy, and the accuracy of the model directly determines the accuracy of the optimized allocation results. Therefore, in-depth research on geometric error modeling methods is particularly important. This article takes the μ2000/800H four-axis horizontal machining center as an example (see Figure 1), which adopts an inverted T-shaped column mobile structure consisting of X, Y, Z translational axes and B rotational axes.

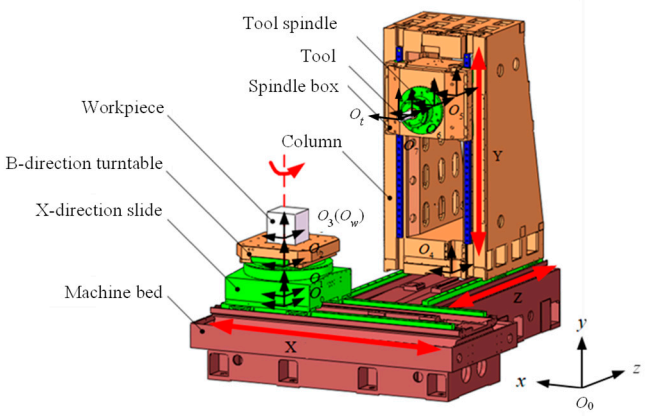

Figure 1. The μ2000/800H horizontal machining center.

In this paper, a general geometric error modeling method based on multi-body system theory is studied. First, the low-order body array is calculated according to the topological structure of the machine tool. Secondly, the characteristic matrix between adjacent bodies is derived by using homogeneous coordinates transformation. Finally, the spatial error model of the whole machine is obtained by applying the motion synthesis principle.

The machine bed is selected as a typical body, and the workpiece kinematic chain is formed in the following order: machine bed, X-direction sliding seat, B-direction turntable, and workpiece. The cutter kinematic chain is established in the order of lathe bed, column, headstock, and spindle. Table 1 presents the low-order body arrays for each component of this multi-body system. L represents the low-order body operator in the low-order body array description method of the multi-body system.

Table 1. Low-order sequence of the μ2000/800H horizontal machining center.

i	0	1	2	3	4	5	6	7
$L^0(i)$	0	1	2	3	4	5	6	7
$L^1(i)$	0	0	1	2	0	4	5	6
$L^2(i)$	0	0	0	1	0	0	4	5
$L^3(i)$	0	0	0	0	0	0	0	4
$L^4(i)$	0	0	0	0	0	0	0	0

The relative position and orientation changes between typical bodies in space can be determined through appropriate transformations of the connected coordinate systems fixed to them, thereby achieving a mathematical description of the multi-body systems. The relative stillness of two adjacent bodies can be considered a state of motion characterized by zero velocity; thus, only the motion transformation of these bodies when relative motion occurs will be examined. According to the principles of dynamics, when analyzing the free motion between two adjacent bodies, it is typically regarded as a combination of translational and rotational motion. This article will employ this approach to investigate the transformation matrix and geometric description of adjacent bodies.

The transformation of position and orientation in space typically employs a homogeneous transformation matrix. For instance, when one body is moving relative to another, the homogeneous transformation matrix that represents its motion characteristics is as follows:

$$\boldsymbol{T}_{ij} = \begin{bmatrix} \boldsymbol{R}_{ij} & \boldsymbol{p}_{ij} \\ 0 & 1 \end{bmatrix} \tag{1}$$

Due to manufacturing and assembly errors in the production process of machine tool components, six types of motion errors can occur when any two adjacent bodies are in relative motion. The free motion between any two adjacent bodies in space can be synthesized through six fundamental motions. Consequently, by understanding the motion error generated by each basic motion, the overall motion error can be determined through motion synthesis. Taking the X-axis and B-axis as examples, the geometric interpretations of the six motion errors associated with their movements are illustrated in Figures 2 and 3.

In general, when the motion axes of the machine tool are in a state of relative static or relative motion, six motion errors will occur. Consequently, the spatial error of the entire machine can be synthesized from the motion errors of each individual axis. For a motion system consisting of $n + 1$ components, we establish corresponding Cartesian coordinate systems $O_i - xyz$ $(i = 0, 1, 2, \cdots, n)$ on all components and set the machine body coordinate system as $O_0 - xyz$, the tool coordinate system as $O - x_t y_t z_t$, and the workpiece coordinate system as $O - x_w y_w z_w$ (see Figure 1).

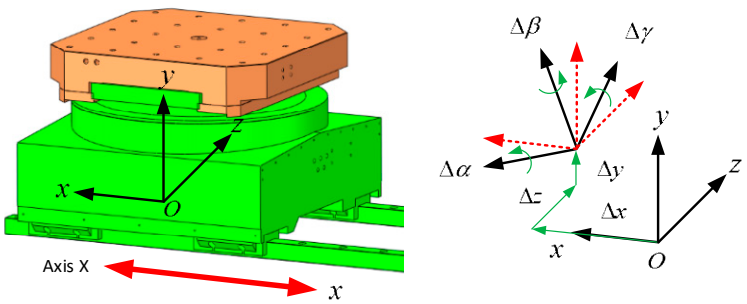

Figure 2. Geometrical significance of six motion errors along the X-axis.

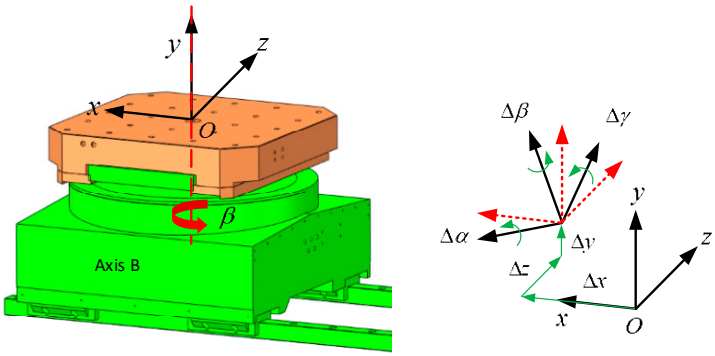

Figure 3. Geometrical significance of six motion errors around the *B*-axis.

Suppose the homogeneous coordinate value of the tool tip in the workpiece coordinate system $O_3 - xyz$ is

$$\boldsymbol{P}_t = \begin{bmatrix} 0 & 0 & t & 1 \end{bmatrix}^T, \tag{2}$$

where t represents the length of the tool.

The homogeneous coordinate value of the tool tip on the tool coordinate system $O_7 - xyz$ is

$$\boldsymbol{P}_w = \begin{bmatrix} x_w & y_w & z_w & 1 \end{bmatrix}^T. \tag{3}$$

Under ideal conditions, the homogeneous coordinate value of the tool point in the bed coordinate system $O_0 - xyz$ is

$$\boldsymbol{P}_{t\_ideal} = \prod_{i=4, L^4(7)=0}^{i=1} \boldsymbol{T}_{L^i(7)L^{i-1}(7)p} \boldsymbol{T}_{L^i(7)L^{i-1}(7)s} \boldsymbol{P}_t, \tag{4}$$

where $\boldsymbol{T}_{L^i(7)L^{i-1}(7)p}$ and $\boldsymbol{T}_{L^i(7)L^{i-1}(7)s}$ represent the ideal translation transformation matrix and the rotation transformation matrix of component i relative to component $i-1$ in the tool kinematic chain, respectively.

The homogeneous coordinate value of the point to be cut on the workpiece in the system $O_0 - xyz$ is

$$\boldsymbol{P}_{w\_ideal} = \prod_{j=3, L^n(3)=0}^{j=1} \boldsymbol{T}_{L^j(3)L^{j-1}(3)p} \boldsymbol{T}_{L^j(3)L^{j-1}(3)s} \boldsymbol{P}_w, \tag{5}$$

where $\boldsymbol{T}_{L^j(3)L^{j-1}(3)p}$ and $\boldsymbol{T}_{L^j(3)L^{j-1}(3)s}$ represent the ideal translation transformation matrix and the rotation transformation matrix of component i relative to component $i-1$ in the workpiece kinematic chain, respectively.

Under ideal conditions, if the tool tip point and the point to be cut on the workpiece coincide, there are

$$\boldsymbol{P}_{t\_ideal} = \boldsymbol{P}_{w\_ideal}. \tag{6}$$

In actual conditions, the homogeneous coordinate value of the tool tip in the $O - x_0y_0z_0$ is

$$\boldsymbol{P}_{t\_actual} = \prod_{i=4, L^n(7)=0}^{i=1} \boldsymbol{T}_{L^i(7)L^{i-1}(7)p} \Delta\boldsymbol{T}_{L^i(7)L^{i-1}(7)p} \boldsymbol{T}_{L^i(7)L^{i-1}(7)s} \Delta\boldsymbol{T}_{L^i(7)L^{i-1}(7)s} \boldsymbol{P}_t, \tag{7}$$

where $\Delta\boldsymbol{T}$ represents the error transformation matrix corresponding to $\boldsymbol{T}$.

The homogeneous coordinate value of the point to be cut on the workpiece in the $O - x_0y_0z_0$ is

$$\boldsymbol{P}_{w\_actual} = \prod_{j=3, L^n(3)=0}^{j=1} \boldsymbol{T}_{L^j(3)L^{j-1}(3)p} \Delta\boldsymbol{T}_{L^j(3)L^{j-1}(3)p} \boldsymbol{T}_{L^j(3)L^{j-1}(3)s} \Delta\boldsymbol{T}_{L^j(3)L^{j-1}(3)s} \boldsymbol{P}_w. \tag{8}$$

Under actual conditions, the difference between the tool tip position and the homogeneous coordinate value of the point to be cut on the workpiece represents the spatial error. Therefore, the spatial error is defined as follows:

$$\Delta \boldsymbol{r} = \boldsymbol{P}_{t\_actual} - \boldsymbol{P}_{w\_actual} = \begin{pmatrix} \Delta X_4 & \Delta Y_4 & \Delta Z_4 & 1 \end{pmatrix}^T \tag{9}$$

where ΔX_4, ΔY_4, and ΔZ_4 represent the position error components of the four-axis machine tool in three directions.

From the spatial error model derived above, it is evident that the spatial error of the entire machine is influenced not only by 29 geometric error sources but also by the machine tool's coordinate position and specific structural parameters [11].

For the aforementioned μ2000/800H, if we consider only the three translational axes X, Y, and Z, without accounting for the rotational *B*-axis movement, it can be simplified into a three-axis horizontal machining center. This configuration involves a total of 21 sources of geometric error. Based on the modeling method discussed in the previous research, the specific derivation process will not be elaborated upon here. It can be concluded that the spatial error of the three-axis horizontal machining center is

$$\Delta \boldsymbol{r} = \boldsymbol{P}_{t\_actual\_3} - \boldsymbol{P}_{w\_actual\_3} = \begin{pmatrix} \Delta X_3 & \Delta Y_3 & \Delta Z_3 & 1 \end{pmatrix}^T, \tag{10}$$

where ΔX_3, ΔY_3, and ΔZ_3 represent the position error components of the three-axis machine tool in three directions.

3. Interval Sensitivity Analysis

Sensitivity refers to the extent to which variations in system input parameters influence changes in the system's response. In the design and manufacturing process, conducting sensitivity analysis on the input parameters is essential for understanding the impact of different inputs on the system's response. This analysis ultimately aids in optimizing the system design methodology.

For a system with input parameters, the response function is denoted as $F(x)$. If $F(x)$ is differentiable, then the first-order sensitivity of the input parameter with respect to $F(x)$ is given by

$$S_i = \frac{\partial F(x)}{\partial x_i}, \ (i = 1, 2, \cdots, n) \tag{11}$$

or

$$S_i = \frac{\Delta F(x)}{\Delta x_i}. \tag{12}$$

According to the definition provided, the first-order sensitivity of the geometric error Δr in the four-axis horizontal machining center to the spatial error of the entire machine is

$$S_i = \frac{\Delta r(e)}{\Delta e_i}. \tag{13}$$

And the error model of the entire machine can be expressed in the following form:

$$\Delta \boldsymbol{r} = \boldsymbol{A}\boldsymbol{e} = \begin{bmatrix} \boldsymbol{A}_\delta & \boldsymbol{A}_\varepsilon \end{bmatrix} \begin{pmatrix} \boldsymbol{e}_\delta & \boldsymbol{e}_\varepsilon \end{pmatrix}^T \tag{14}$$

where $\Delta \mathbf{r} = \begin{pmatrix} \Delta X & \Delta Y & \Delta Z \end{pmatrix}^T$ represents the spatial error between the tool tip point and the point to be cut on the workpiece, $\boldsymbol{A}$ represents the corresponding error-mapping matrix, $\boldsymbol{e}$ represents the geometric error source vector, $\boldsymbol{A}_\delta$ and $\boldsymbol{A}_\varepsilon$ represent the corresponding error mapping matrix, and $\boldsymbol{e}_\delta(\boldsymbol{e}_\varepsilon)$ represents the positional (angular) error source vector.

The elements in $\boldsymbol{A}_\varepsilon$ are the function of the coordinates of machine tool motion, $\boldsymbol{A}_\varepsilon^{(x,y,z,t)}$ can be used to represent the error mapping matrix corresponding to the angular error source of the machine tool motion parameters (x, y, z, t). Then, the interval expansion factor from the mth angle error source $[e_{\varepsilon m}]$ to the ith spatial error component $[\Delta r_i]$ is

$$\eta_{\varepsilon im}{}^{(x,y,z,t)} = A_{\varepsilon im}{}^{(x,y,z,t)}. \tag{15}$$

In precision machine tools, manufacturing and installation errors in the guide rails can lead to angular errors when moving parts traverse along the axis. Consequently, these angular errors generate position error components at any point within the processing space. This position error component is referred to as an Abbe error. Figure 4 illustrates the Abbe error resulting from the pitch angle of the X-axis. It is important to note that the factor influencing the accuracy design of the machine tool is $\varepsilon_z(x)\cdot y$ rather than the machining error $\varepsilon_z(x)\cdot\eta^{(x,y,z,t)}$ that occurs in the X-axis direction. Therefore, when considering the sources of angular error, the presence of Abbe error indicates that the interval expansion factor cannot be employed directly as a measure of sensitivity. Based on these considerations, we define the sensitivity $S_{\varepsilon im}$ of the angular error $[e_{\varepsilon m}]$ to the spatial error component $[\Delta r_i]$ as follows:

$$S_{\varepsilon im} = \eta_{\varepsilon im}^{(x,y,z,t)} - \eta_{\varepsilon im}^{(0,0,0,0)} \tag{16}$$

where $\eta_{\varepsilon im}^{(0,0,0,0)}$ is the interval expansion factor from the mth angle error $[e_{\varepsilon m}]$ to the ith spatial error component $[\Delta r_i]$ when the three axes are located at the origin and the tool length is 0.

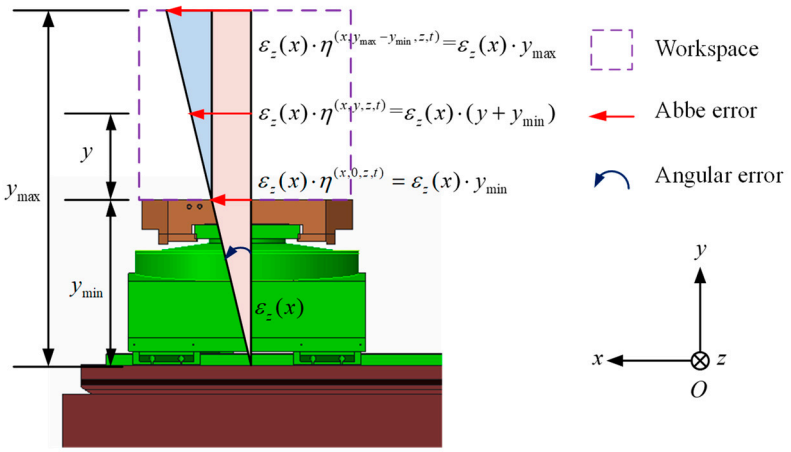

Figure 4. Abbe errors caused by the pitch angle of the X-axis.

The global maximum interval sensitivity $S_{\varepsilon im}^*$ of the angle error $[e_{\varepsilon m}]$ to the spatial error component $[\Delta r_i]$ is defined as

$$S_{\varepsilon im}^* = \max(S_{\varepsilon im}). \tag{17}$$

The global maximum interval sensitivity S_j^* of the jth geometric error to spatial error is defined as follows:

$$S_j^* = \sqrt{\sum_{i=1}^{3} S_{ij}^{*2}}\ (j = 1, 2, \cdots, 21). \tag{18}$$

The global maximum interval sensitivity S_j^*, as defined above, can be directly utilized as the sensitivity design index for machine tool accuracy. Utilizing this sensitivity design index, the tolerance domain for each error, derived from its distribution, can satisfy the

design index requirements for all geometric errors across the entire workspace of the machine tool.

According to the structural parameters of the machine tool, the spatial error model is simplified, and the interval sensitivity analysis is conducted in the machining space $V = X \times Y \times Z$, which is composed of the X, Y, and Z axes.

The interval sensitivity of the six geometric errors of the *X*-axis to the spatial error can be calculated using Equations (16)–(18). Figure 5 illustrates the graphical representation of the interval sensitivity.

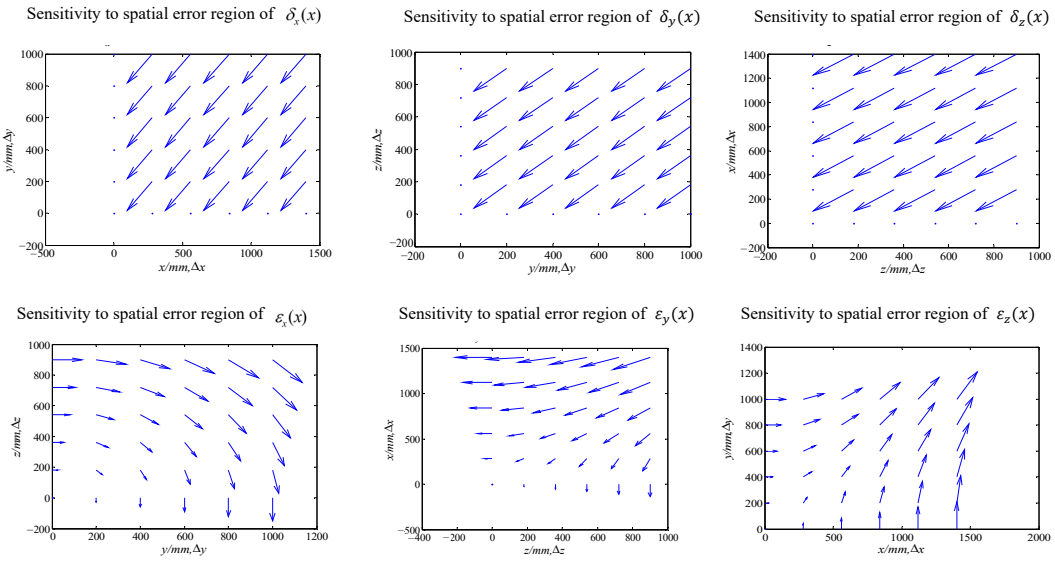

Figure 5. Graphical representation of interval sensitivity.

From Figure 5, it is evident that the six geometric errors of the *X*-axis all influence the spatial errors; however, their effects do not exhibit a consistent pattern. The global maximum interval sensitivity of each geometric error source to spatial error can be calculated using Equation (18), as shown in Figure 6.

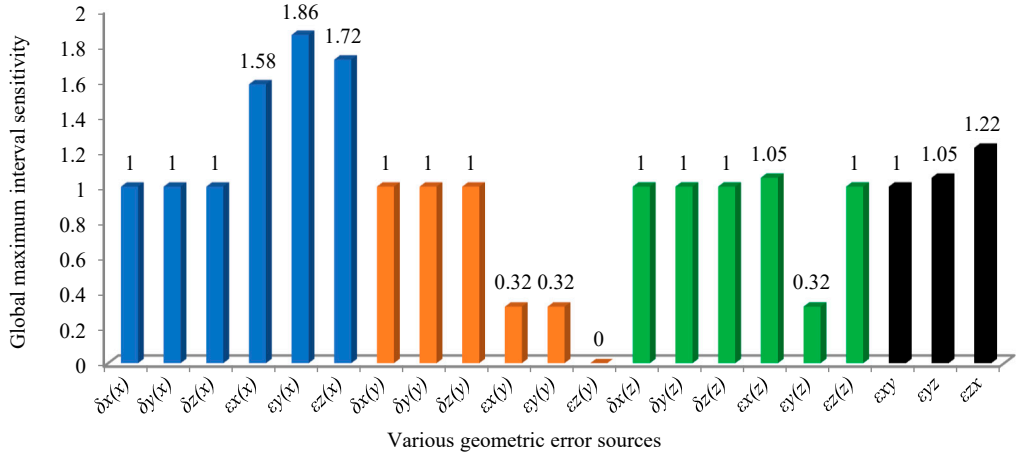

Figure 6. Global maximum interval sensitivity to spatial error of geometric error sources.

Figure 6 illustrates the results of the global maximum interval sensitivity analysis for each geometric error to spatial error. The blue, orange, and green sections represent the global maximum interval sensitivities of the six geometric errors of the *X*-, *Y*-, and *Z*-axis, respectively. Additionally, the black section denotes the maximum sensitivity of the perpendicularity errors of the three translational axes to spatial errors across the entire

workspace. Except for $\varepsilon_z(y)$ during the movement of the spindle box, which does not affect the spatial error, all other geometric errors have varying degrees of impact on the maximum sensitivity of the spatial error region.

In the following process of allocating tolerances, it is essential to strictly control the tolerance range of geometric errors that exhibit high sensitivity to the maximum range of spatial errors. Conversely, for geometric errors that demonstrate low sensitivity to the maximum range of spatial errors, the tolerance range can be relaxed appropriately.

4. Optimized Allocation of Geometric Accuracy

4.1. Interval Optimization Model

Based on the spatial error model established in the previous section, twenty-one geometric errors are utilized as design variables. These design variables are defined as x_1 through x_{21}, corresponding to the *X*-axis, *Y*-axis, *Z*-axis, and perpendicularity.

By internalizing the above 21 design variables, it can be obtained that

$$[\boldsymbol{X}] = \{[x_1], [x_2], \cdots, [x_{21}]\}, \tag{19}$$

where $[x_i] = [0, \overline{x_i}]$ $(i = 1, 2, \cdots, 21)$. For example, the interval representation of $\delta_x(y) = 6$ μm/m is $\delta_x(y) \in [0, 6]$, which means that when the spindle box moves throughout its full stroke, the range of straightness error in the X-direction is 0~6 μm/m, with a maximum value of 6 μm/m.

According to research on the optimal allocation of geometric accuracy, the current mainstream methods include the mean squared error allocation method and the tolerance–cost model allocation method. When the mean squared error distribution method is employed to optimize geometric accuracy distribution, some error terms may be excessively lenient while others may be overly stringent. Conversely, when utilizing the tolerance–cost model allocation method to enhance geometric accuracy, it is essential to select the appropriate tolerance–cost functions based on various machining features. These tolerance–cost functions are derived from engineering experience or extensive experimentation under specific conditions, which limits their versatility and accuracy.

In order to address the limitations of the two methods mentioned above, this paper utilizes the global maximum interval sensitivity of each geometric error as a weighting factor. The design objective is to maximize the sum of the products of the interval width of each geometric error source and its corresponding global maximum interval sensitivity. The objective function is defined as follows:

$$\max f([\boldsymbol{X}]) = \sum_{i=1}^{21} S_i^* d([x_i]),\ (i = 1, 2, \cdots, 21) \tag{20}$$

where $[\boldsymbol{X}] = \{[x_1], [x_2], \cdots, [x_{21}]\}$ is the interval vector of the design variables, S_i^* is the global maximum interval sensitivity of geometric errors to the spatial error, and $d([x_i])$ is the interval width of the geometric error.

In the traditional forward design process of geometric accuracy of CNC machine tools, the allowable variation range of positioning errors of the three translational axes is usually used as the constraint condition of tolerance allocation. This method ignores the correlation between the errors of each axis, resulting in tolerance allocation results that cannot meet the requirements of machine tool accuracy design. Therefore, the allowable variation range of the position error of the tool tip relative to the workpiece is regarded as a sphere in this paper. As long as the error falls within the sphere, it is considered that the accuracy of the machine tool meets the design requirements. According to the actual working conditions, the spatial error constraint for the entire machine is established: the deviation of the overall

spatial geometric error in the body diagonal positioning system, within 60% of the working space, must not exceed 25 μm.

Figure 7a illustrates the diagonal space error diagram of the entire system. Within the workspace, there are four diagonal lines, *ppp*, *npp*, *pnp*, and *ppn*, where *p* represents the forward direction and *n* represents the reverse direction, as depicted in Figure 7a. Taking the body diagonal *ppp* as an example, the machine tool is configured to measure the spatial error along this diagonal. Due to the presence of spatial error, the ideal measurement point does not align with the actual measurement point, as shown in Figure 7b. Geometrically, the spatial error constraint of the machine tool can be defined as a spherical envelope surface with an ideal measurement point as the center and a radius R of 12.5 μm. When the modulus of the spatial error vector $\Delta \boldsymbol{r}$ is less than or equal to R, the actual measurement point is qualified, such as the point p_{a1}; when the modulus of the spatial error vector $\Delta \boldsymbol{r}$ is greater than R, it shows that the actual measurement point is out of tolerance, such as the point p'_{a1}. Therefore, the constraint condition of the spatial error can be defined as

$$\Delta r = \sqrt{\Delta x^2 + \Delta y^2 + \Delta z^2} \leq R = 12.5, \tag{21}$$

where Δr is the modulus of the spatial error vector $\Delta \boldsymbol{r}$ and Δx, Δy, and Δz are the error components in the X, Y, and Z directions, respectively.

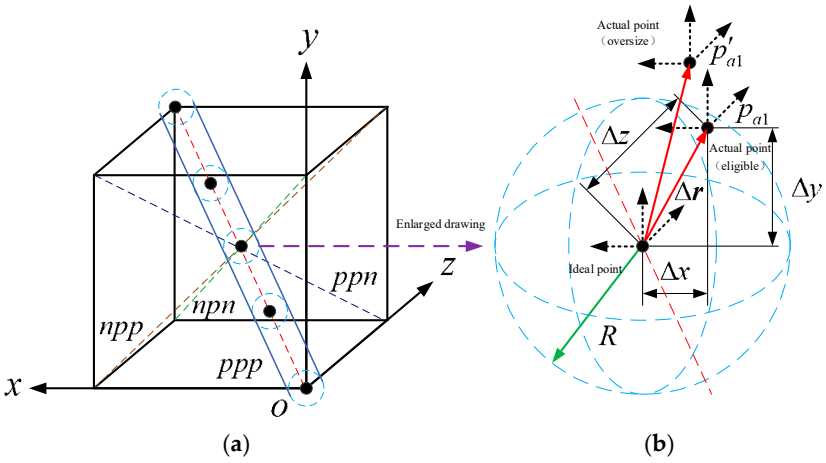

Figure 7. Volumetric error along the body diagonals of the whole workspace. (**a**) Measuring space and four body diagonals; (**b**) local amplification diagram of the measuring point.

The geometric accuracy of the machine tool is primarily determined by the precision of its components and the accuracy of its assembly. During actual manufacturing and installation, cumulative errors from screw pitch and unavoidable manufacturing and installation errors of the guide rail prevent each geometric error source interval from reaching an ideal state, meaning that $\overline{x_i} > 0$. Consequently, it is crucial to carefully select the constraint range for the upper bound of each geometric error source interval to optimize the results of geometric accuracy allocation.

According to error traceability technology, we can establish the relationship between geometric error sources and the accuracy parameters of the associated components. The relevant expressions are presented in Tables 2–4.

Table 2. Corresponding relationships between the position error sources and the accuracy parameters.

Positioning Error	Horizontal Straightness Error	Vertical Straightness Error
$x_1 = \delta_x(x) = S(x)$	$x_3 = \delta_z(x) = \Delta s_1(x)$	$x_2 = \delta_y(x) = \Delta s_2(x)$
$x_7 = \delta_y(y) = S(y)$	$x_8 = \delta_x(y) = \Delta s_1(y)$	$x_9 = \delta_z(y) = \Delta s_2(y)$
$x_{13} = \delta_z(z) = S(z)$	$x_{14} = \delta_x(z) = \Delta s_1(z)$	$x_{15} = \delta_y(z) = \Delta s_2(z)$

Table 3. Corresponding relationships between the angular error sources and the accuracy parameters.

Roll Angular Error	Pitch Error	Yaw Error
$x_4 = \varepsilon_x(x) = \Delta s_3(x)$	$x_6 = \varepsilon_z(x) = \Delta s_2(x)/l(x)$	$x_5 = \varepsilon_y(x) = \Delta s_1(x)/l(x)$
$x_{11} = \varepsilon_y(y) = \Delta s_3(y)$	$x_{10} = \varepsilon_x(y) = \Delta s_2(y)/l(y)$	$x_{12} = \varepsilon_z(y) = \Delta s_1(y)/l(y)$
$x_{18} = \varepsilon_z(z) = \Delta s_3(z)$	$x_{16} = \varepsilon_x(z) = \Delta s_2(z)/l(z)$	$x_{17} = \varepsilon_y(z) = \Delta s_1(z)/l(z)$

Table 4. Corresponding relationships between perpendicularity errors and accuracy parameters.

Perpendicularity Error	Calculation Expression
XY perpendicularity error	$x_{19} = \varepsilon_{xy} = \text{arctg}(\Delta s_2(x)/l(x)) - \text{arctg}(\Delta s_1(y)/l(y))$
YZ perpendicularity error	$x_{20} = \varepsilon_{yz} = \text{arctg}(\Delta s_2(y)/l(y)) - \text{arctg}(\Delta s_2(z)/l(z))$
ZX perpendicularity error	$x_{21} = \varepsilon_{zx} = \text{arctg}(\Delta s_1(z)/l(z)) - \text{arctg}(\Delta s_1(x)/l(x))$

Combining Equations (19)–(21), standard interval optimization models can be established. The interval operation rules and interval expansion theorem are used to simplify the above interval optimization models, and the following specific forms can be obtained.

Solve $\boldsymbol{X} = \{\overline{x_1}, \overline{x_2}, \cdots, \overline{x_{21}}\}$, and

$$\begin{aligned} &\min f(\boldsymbol{X}) = \sum_{i=1}^{n} S_i^*(\overline{x_i})^{-2} \\ &s.t.\ \sqrt{\Delta x^2 + \Delta y^2 + \Delta z^2} - 12.5 \le 0 \\ &\quad lb(\overline{x_i}) \le \overline{x_i} \le ub(\overline{x_i}) \\ &\quad \boldsymbol{X} = \{\overline{x_1}, \overline{x_2}, \cdots, \overline{x_{21}}\} \\ &\quad i = 1, 2, \cdots, n \end{aligned} \quad . \tag{22}$$

4.2. Solving the Interval Optimization Model Based on the Genetic Algorithm

For the optimization problem described in Equation (22), the objective function is nonlinear, the constraints include both linear and nonlinear components, and there are multiple design variables, which contribute to the complexity of the optimization model. Due to its inherent heuristic random search characteristics, robust parallel computing capabilities, and independence from auxiliary information, the genetic algorithm (GA) is well suited for efficiently and accurately solving the aforementioned optimization problems. Consequently, this article employs the genetic algorithm to address the optimization problem outlined in Equation (22).

This article is based on the MATLAB R2016b genetic algorithm toolbox to solve interval optimization models, with specific parameter settings as follows:

(1) Population size N: The rate of convergence of the genetic algorithm depends on the size of the population. If the scale is too small, it is easy to converge to the local optimal solution; if the population is too large, the rate of convergence will be reduced. Generally, 10~20 will be selected. In this paper, N = 10 is selected.

(2) Variable dimension n: There are a total of 21 design variables in the interval optimization model to be solved in this article, so n = 21 is selected.

(3) Binary encoding length M: This article adopts binary encoding and sets the interval of the ith design variable as $[a_i, b_i]$, requiring an accuracy of 10^{-6}. The binary encoding length of a certain design variable can be obtained through Equation (23):

$$2^{m_i-1} \leq (b_i - a_i) \times 10^6 \leq 2^{m_i} - 1. \tag{23}$$

The total binary encoding length M is

$$M = \sum_{i=1}^{21} m_i. \tag{24}$$

(4) Crossover rate p_c: Parent individuals generate corresponding offspring individuals through crossover operations. If the crossover rate is too small, search operations can easily lead to stagnation; if the crossover rate is too high, the intergenerational crossover is more sufficient, but it is easy to damage the excellent individuals in the population. The recommended value range for p_c is generally 0.4~0.99, and in this article, p_c = 0.8 is selected.

(5) Variation rate p_m: Setting the variation rate reasonably can effectively avoid premature puberty. If the mutation rate is too high, it increases individual diversity, but some excellent individuals may be destroyed; if the mutation rate is too small, the individual is relatively stable, but the possibility of premature puberty and falling into local optimization greatly increases. It is generally recommended that the value range of p_m is 0.0001~0.1, and in this article, p_m = 0.08 is selected.

(6) Cutoff condition: Define the maximum genetic algebra G as the cutoff condition, and this article selects G = 100.

From Equation (18), it can be seen that the three components in the constraint inequality are not only related to the 21 geometric error sources (design variables), but also to the machine tool coordinates. Therefore, to find the optimal solution for 21 design variables, it is necessary to concretize the machine tool coordinates. Ten equidistant feature space points are taken on a diagonal line of the working space of the machining tool, and the specific coordinate values are shown in Table 5. In the table, groups 1 to 10 indicate that the machine tool workbench tends toward the leftmost end, the spindle box tends toward the uppermost end, and the column tends toward the rearmost end.

Table 5. Coordinate of the characteristic points of the workspace body diagonal.

Group	**1**	**2**	**3**	**4**	**5**	**6**	**7**	**8**	**9**	**10**
X/mm	−1400	−1260	−1120	−980	−840	−700	−560	−420	−280	−140
Y/mm	−1000	−900	−800	−700	−600	−500	−400	−300	−200	−100
Z/mm	−900	−820	−740	−660	−580	−500	−420	−340	−260	−180

Run the genetic algorithm toolbox, set the above determined genetic algorithm parameters, and obtain 10 sets of optimal solutions, as shown in Figure 8.

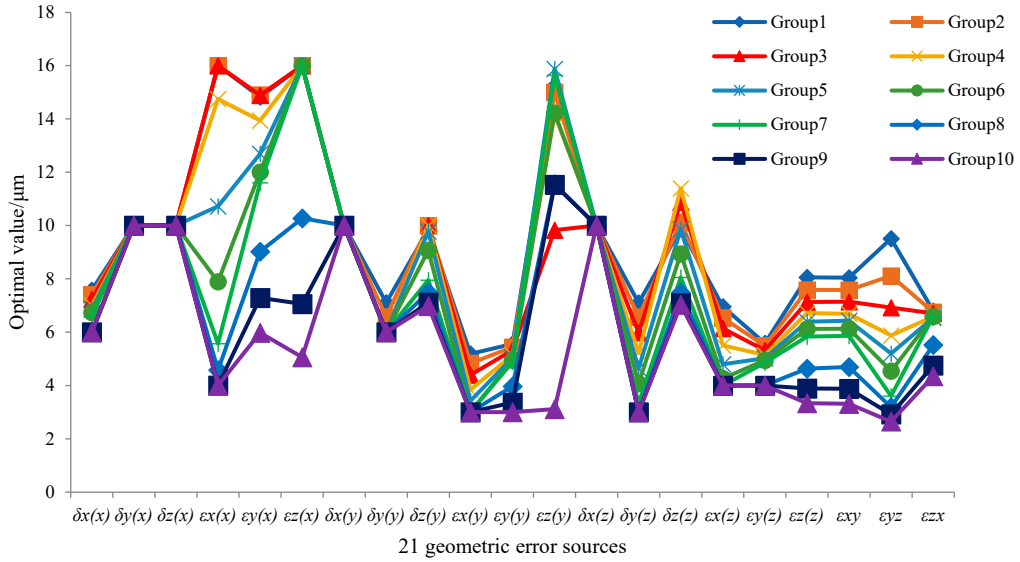

Figure 8. Shown are 10 sets of optimization values of 21 geometric error sources.

It can be seen that the optimized allocation values of the 21 geometric error sources are related to the machine tool coordinates. Specifically, as the machine tool workbench tends toward the leftmost end, the spindle box tends toward the uppermost end, and the column tends toward the rearmost end. Furthermore, the optimized values of each geometric error source become smaller and smaller; that is, the accuracy requirements of each geometric error source become increasingly strict. The change in the optimized value of the angle error source is more significant than that of the position error source. This is due to the existence of Abbe error. As the motion distance of each axis of the machine tool increases, the position error component caused by Abbe error in the workspace increases, leading to increasingly strict accuracy requirements for various geometric error sources. Taking the minimum of 10 sets of optimization values as the final optimization allocation value for each geometric error source can ensure that the solved geometric error optimization values meet the accuracy allocation requirements throughout the entire workspace. The accuracy allocation results for 21 geometric error sources are shown in Tables 6–9.

Table 6. The accuracy distribution results for six geometric errors of the *X*-axis.

Variables	x_1 μm	x_2 μm	x_3 μm	x_4 μm/m	x_5 μm/m	x_6 μm/m
Error source	$\delta_x(x)$	$\delta_y(x)$	$\delta_z(x)$	$\varepsilon_x(x)$	$\varepsilon_y(x)$	$\varepsilon_z(x)$
Optimal values	6	10	10	4	5.979	5.061

Table 7. The accuracy distribution results for six geometric errors of the *Y*-axis.

Variables	x_7 μm	x_8 μm	x_9 μm	x_{10} μm/m	x_{11} μm/m	x_{12} μm/m
Error source	$\delta_x(y)$	$\delta_y(y)$	$\delta_z(y)$	$\varepsilon_x(y)$	$\varepsilon_y(y)$	$\varepsilon_z(y)$
Optimal values	10	6	6.984	3	3	3.113

Table 8. The accuracy distribution results for six geometric errors of the *Z*-axis.

Variables	x_{13} μm	x_{14} μm	x_{15} μm	x_{16} μm/m	x_{17} μm/m	x_{18} μm/m
Error source	$\delta_x(z)$	$\delta_y(z)$	$\delta_z(z)$	$\varepsilon_x(z)$	$\varepsilon_y(z)$	$\varepsilon_z(z)$
Optimal values	10	3	7.027	4	4	3.334

Table 9. The accuracy distribution results for verticality errors of the vertical axis.

Variables	x_{19} **μm/m**	x_{20} **μm/m**	x_{21} **μm/m**
Error source	ε_{xy}	ε_{yz}	ε_{zx}
Optimal values	3.312	2.651	4.35

4.3. Comparison of Geometric Accuracy Optimization Allocation Results with Theoretical Values

The above geometric accuracy optimization allocation results based on the genetic algorithm solution did not consider the error homogenization effect. In order to compare and analyze the obtained geometric accuracy optimization allocation results with the theoretical values considering the error homogenization effect, taking the *X*-axis assembly process as an example, the guide rail error homogenization coefficient is obtained without considering the error homogenization effect, and then the quantitative relationship between the optimized geometric accuracy allocation value and the theoretical value is studied.

Figure 9 shows the measurement process of the vertical straightness error and pitch angle error of the *X*-axis guide rail. The measuring instrument is an ultra-precision autocollimator with a resolution of 0.1 μm/mm. During the error measurement process, the autocollimator reflector is fixed on the slider, and the total measurement distance is divided into 12 planes based on the length of the slider. Each time the slider moves one plane in front of another, a total of 13 data points are measured. The measurement results of the vertical straightness error and pitch angle error of the guide rail are shown in Figures 10 and 11, respectively.

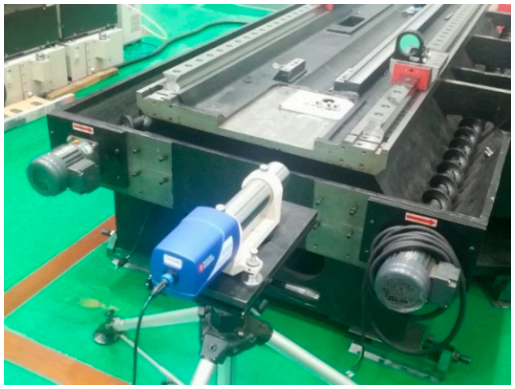

Figure 9. Measurement for *X*-axis guide error of the μ2000/800H horizontal machining center.

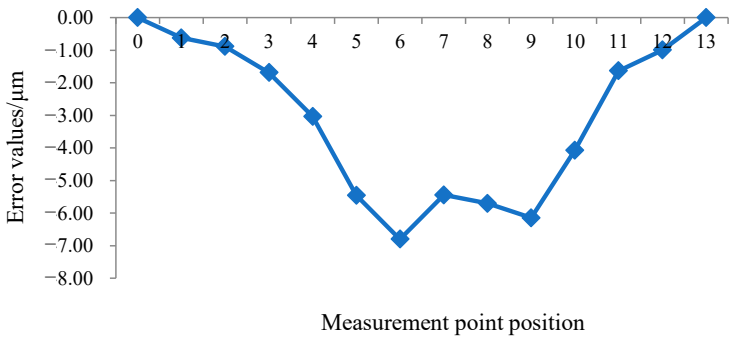

Figure 10. Measurement results for vertical straightness error of *X*-axis.

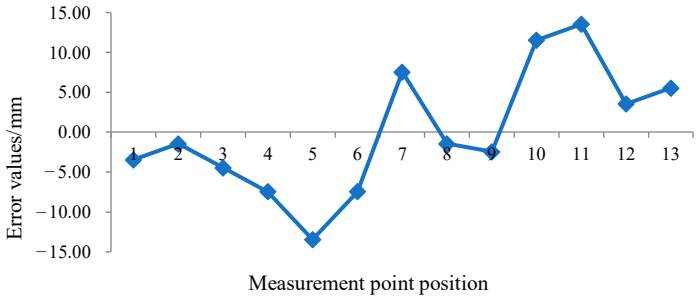

Figure 11. Measurement results for pitch error of *X*-axis.

From Figures 10 and 11, it can be seen that the measured vertical straightness error of the *X*-axis guide rail is 6.8 μm. The pitch angle error is 27 μm/mm.

Figure 12 shows the measurement process of the comprehensive vertical straightness error and pitch angle error of the *X*-axis workbench of the machining center. The measuring instruments also use ultra-precision autocollimators. In the process of error measurement, the autocollimator reflector is fixed at the Centroid of the upper end face of the workbench. According to the length of the workbench, the total measurement travel is divided into 8 intervals. Each time, the corresponding slider moves 1 level head to tail, and a total of 9 data points are measured. The measurement results of the vertical straightness error and pitch angle error of the guide rail are shown in Figures 13 and 14, respectively.

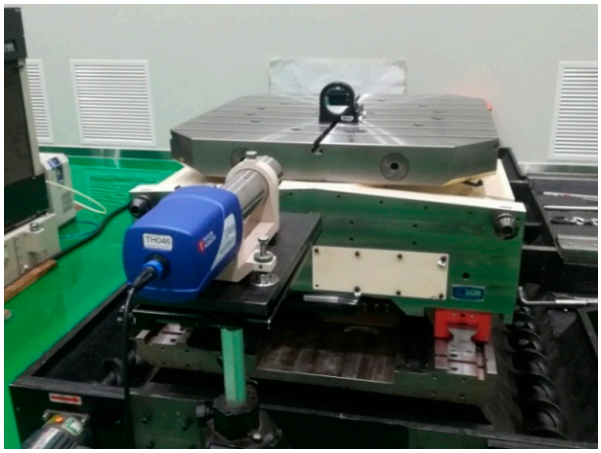

Figure 12. Measurement for *X*-axis integrated error of the μ2000/800H horizontal machining center.

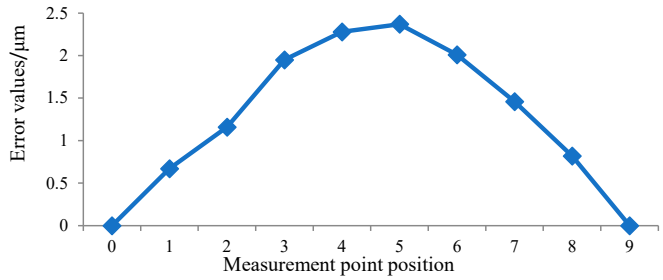

Figure 13. Measurement results for integrated vertical straightness error of the *X*-axis.

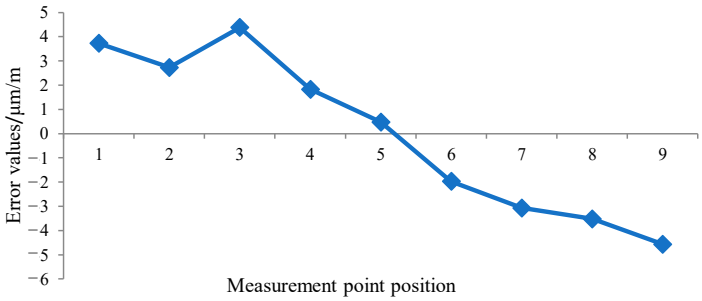

Figure 14. Measurement results for integrated pitch error of the *X*-axis.

From Figures 13 and 14, it can be seen that the measured comprehensive vertical straightness error of the *X*-axis workbench is 2.37 μm. The comprehensive pitch angle error is 8.95 μm/mm.

According to the definition of error averaging coefficient $n_e = E_w/e_g$ (E_w is the motion error of the moving component, e_g is the geometric error of the guide rail), the average coefficient of the *X*-axis vertical straightness error is 0.35, and the average coefficient of the pitch angle error is 0.33. For the convenience of research, this article uniformly takes an error averaging coefficient of about 1/3. The theoretical values without considering the error homogenization effect can be obtained by using this error homogenization coefficient. Tables 10–13 show the comparison between the geometric accuracy optimization allocation values solved in this paper and the theoretical values.

Table 10. Comparison of accuracy distribution results with theoretical value for six geometric errors of the *X*-axis.

Error Source	$\delta_x(x)$ μm	$\delta_y(x)$ μm	$\delta_z(x)$ μm	$\varepsilon_x(x)$ μm/m	$\varepsilon_y(x)$ μm/m	$\varepsilon_z(x)$ μm/m
Actual allocated value	6	10	10	4	5.979	5.061
Theoretical design value	2	1.667	1.667	2.667	2.667	2.667
Difference	4	8.333	8.333	1.333	3.312	2.394

Table 11. Comparison of accuracy distribution results with theoretical value for six geometric errors of the *Y* axis.

Error Source	$\delta_x(y)$ μm	$\delta_y(y)$ μm	$\delta_z(y)$ μm	$\varepsilon_x(y)$ μm/m	$\varepsilon_y(y)$ μm/m	$\varepsilon_z(y)$ μm/m
Actual allocated value	10	6	6.984	3	3	3.113
Theoretical design value	1.667	2	1.667	2.667	2.667	2.667
Difference	8.333	4	5.317	0.333	0.333	0.446

Table 12. Comparison of accuracy distribution results with theoretical value for six geometric errors of the *Z* axis.

Error Source	$\delta_x(z)$ μm	$\delta_y(z)$ μm	$\delta_z(z)$ μm	$\varepsilon_x(z)$ μm/m	$\varepsilon_y(z)$ μm/m	$\varepsilon_z(z)$ μm/m
Actual allocated value	10	3	7.027	4	4	3.334
Theoretical design value	1.667	1.667	2	2.667	2.667	2.667
Difference	8.333	1.333	5.027	1.333	1.333	0.667

Table 13. Comparison of accuracy distribution results with theoretical value for verticality errors of the vertical axis.

Error Source	ε_{xy} μm/m	ε_{yz} μm/m	ε_{zx} μm/m
Actual allocated value	3.312	2.651	4.35
Theoretical design value	3.333	3.333	3.333
Difference	−0.021	−0.682	1.017

According to the comparison between the geometric accuracy allocation values and the theoretical values in Tables 10–13, it can be seen that the allocation values of geometric accuracy, except for perpendicularity error ε_{xy} and ε_{yz}, have become tighter by 0.021 μm/m and 0.682 μm/m. The allocation values of the other 19 geometric accuracy items have achieved varying degrees of relaxation.

Based on the geometric accuracy allocation results obtained above, 1000 spatial points are randomly selected in the workspace for simulation verification. When each geometric error is the fixed value x_i, 1000 estimated values of spatial errors are obtained by substituting them into the spatial error model. The distribution is shown in Figure 15, with 989 qualified points and 11 exceedances. The frequency distribution histogram is shown in Figure 16, and the estimated spatial error values are mainly distributed between 6.5 and 11 μm. The design accuracy satisfaction rate reaches 98.9%.

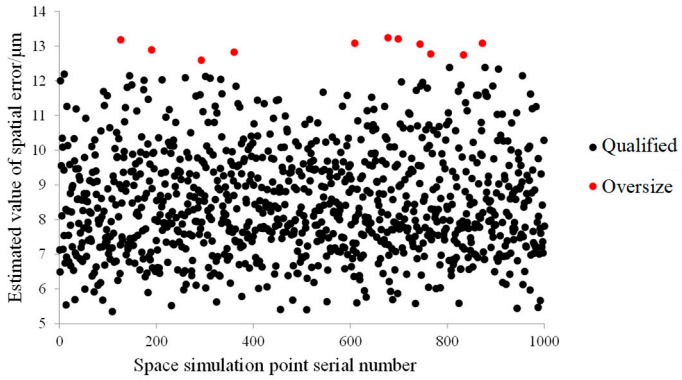

Figure 15. The scatter plot of the spatial error estimated value with definite geometric error.

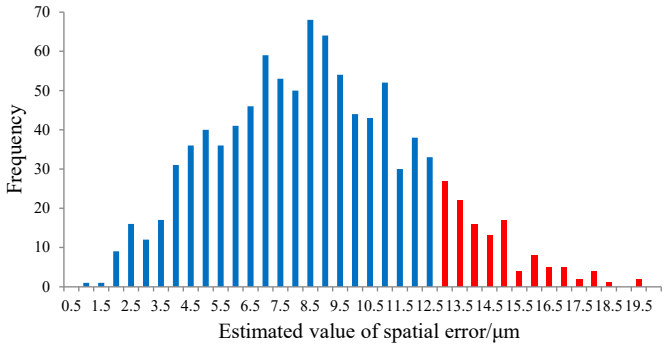

Figure 16. The frequency distribution histogram of the spatial error estimated value with stochastic geometric error.

Through the simulation of spatial error prediction in the above two cases, the rationality of the accuracy distribution results of each geometric error source of the machine tool and the correctness of the accuracy optimization distribution method studied in this paper are verified. Figure 17 shows the design range of each geometric error source. The red

value represents the accuracy range of the position error source, the black value represents the accuracy range of the angle error source, and the red envelope line represents the upper limit of the accuracy range value. Based on the above research, it can be concluded that in the actual process of machine tool design and manufacturing, if the design indicators given by each geometric error source are within the red envelope, it can be considered that the design indicators given by each geometric error source meet the accuracy design requirements of the entire machine with an accuracy satisfaction rate of 87.4%.

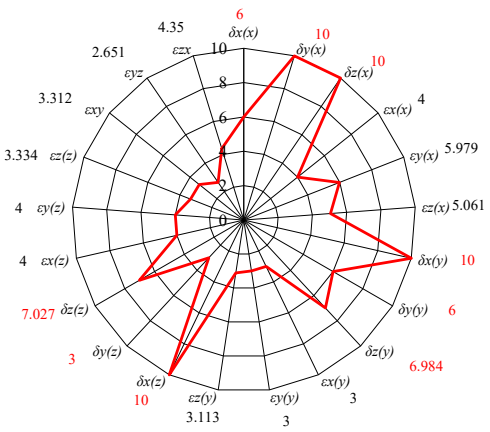

Figure 17. The designed tolerance of each geometric error.

5. Conclusions

This study systematically investigates a method for optimizing geometric accuracy allocation in precision horizontal machining centers utilizing interval theory. A comprehensive spatial error model for machine tools is developed based on multi-body system theory. By employing homogeneous coordinate transformations, the study derives the ideal static matrix, ideal motion matrix, static error matrix, and motion error matrix under both ideal and actual motion conditions. The overall spatial error model is subsequently obtained through the multiplication of these kinematic matrices.

The research further explores interval sensitivity analysis techniques grounded in interval theory, defining interval expansion factors. It incorporates considerations of Abbe error, defining the interval sensitivity of positional error sources, angular error sources, and the maximum interval sensitivity across the entire workspace. The interval optimization model utilizes the interval widths of 21 geometric errors as design variables, while imposing a constraint that the deviation of the diagonal position must not exceed 25 μm. Additionally, the maximum sensitivity across the entire workspace of these 21 geometric errors is considered to be the weighting factor. The primary objective of the design is to maximize the interval widths of the 21 geometric errors. This study employs a genetic algorithm to address the interval optimization model. Following the precision allocation outcomes, a simulation verification is performed for each source of geometric error, utilizing both fixed and interval values. The compliance rates for spatial accuracy are determined to be 98.9% and 87.4%, respectively. These findings substantiate the validity of the tolerance allocation results. Compared with the existing machine tool accuracy design methods, the tolerance allocation strategy proposed in this paper not only considers the coupling design between the errors in all directions, but also reduces the manufacturing cost under the premise of ensuring the spatial accuracy of the whole machine.

The forward design method of geometric accuracy of CNC machine tools proposed in this paper is obtained under the assumption that the error sources are independent of each other. In the follow-up study, the correlation between errors and the influence of thermal errors will be further considered.

Author Contributions: Conceptualization, W.T. and D.Z.; data curation, L.W. and X.L.; formal analysis, L.W. and X.L.; funding acquisition, L.W. and W.T.; investigation, W.T.; methodology, W.T.; project administration, W.T.; resources, D.Z.; software, L.W. and X.L.; supervision, D.Z.; validation, L.W., X.L., and W.T.; visualization, L.W. and X.L.; writing—original draft, L.W.; writing—review and editing, W.T. All authors have read and agreed to the published version of the manuscript.

Funding: This work was supported by the Research Plan Projects of Tianjin Education Commission (Grant 2023KJ249) and National Science and Technology Major Projects (Grant 2024ZD0708801).

Data Availability Statement: Data are contained within the article.

Conflicts of Interest: The authors declare no conflicts of interest.

References

1. Sheng, B.H.; Tang, H. Comprehensive Dynamic Compensation Technology for Errors in CNC Machine Tools. *Manuf. Technol. Mach. Tools* **1997**, *6*, 19–21.
2. Denavit, J.; Hartenberg, R.S. A kinematic notation for lower-pair mechanisms based on matrices. *J. Appl. Mech.* **1955**, *22*, 215–221. [CrossRef]
3. Leete, D.L. Automatic compensation of alignment errors in machine tools. *Int. J. Mach. Tool Des. Res.* **1961**, *1*, 293–324. [CrossRef]
4. French, D.; Humphries, S.H. Compensation for backlash and alignment errors in a numerically controlled machine tool by a digital computer program. In Proceedings of the 8th International MTDR Conference, Manchester, UK, 11–15 September 1967; pp. 167–172.
5. Ferreira, P.M.; Liu, C.R. An analytical quadratic model for the geometric error of a machine tool. *Trans. ASME J. Manuf. Syst.* **1986**, *5*, 51–63. [CrossRef]
6. Yang, J.G.; Pan, Z.H.; Xue, B.Y. Kinematics Modeling of Geometric and Thermal Error Synthesis of CNC Machine Tools. *Mech. Des. Manuf.* **1998**, *5*, 31–32.
7. Lin, P.D.; Ehmann, K.F. Direct volumetric error evaluation for multi-axis machines. *Int. J. Mach. Tools Manuf.* **1993**, *33*, 675–693. [CrossRef]
8. Reshetov, D.N.; Portman, V.T. *Accuracy of Machine Tools*; ASME Press: New York, NY, USA, 1988.
9. Wu, Y.C.; Shen, J. Volumetric error modeling and accuracy improvement by parameter identification of a compound machine tool. *J. Adv. Mech. Des. Syst. Manuf.* **2021**, *15*, 0065. [CrossRef]
10. Díaz-Tena, E.; Ugalde, U.; López de Lacalle, L.N.; De la Iglesia, A.; Calleja, A.; Campa, F.J. Propagation of assembly errors in multitasking machines by the homogenous matrix method. *Int. J. Adv. Manuf. Technol.* **2013**, *68*, 149–164. [CrossRef]
11. Tian, W.J.; Gao, W.G.; Zhang, D.W.; Huang, T. A general approach for error modeling of machine tools. *Int. J. Mach. Tools Manuf.* **2014**, *79*, 17–23. [CrossRef]
12. Tao, H.; Fan, J.; Li, T.; Chen, F.; Pan, R. An approach to enhancing machining accuracy of five-axis machine tools based on a new sensitivity analysis method. *Int. J. Adv. Manuf. Technol.* **2023**, *124*, 2383–2400. [CrossRef]
13. Olvera, D.; López de Lacalle, L.N.; Compeán, F.I.; Fz-Valdivielso, A.; Lamikiz, A.; Campa, F.J. Analysis of the tool tip radial stiffness of turn-milling centers. *Int. J. Adv. Manuf. Technol.* **2012**, *60*, 883–891. [CrossRef]
14. Iigo, B.; Colinas-Armijo, N.; López de Lacalle, L.N.; Aguirre, G. Digital twin-based analysis of volumetric error mapping procedures. *Precis. Eng.* **2021**, *72*, 823–836.
15. Song, L.; Sun, T.; Jia, R.; Liu, H.; Zhao, X. An error allocation method for five-axis ultra-precision machine tools. *Int. J. Adv. Manuf. Technol.* **2024**, *130*, 2601. [CrossRef]
16. Karamchandani, A.; Cornell, C.A. Sensitivity estimation within first and second order reliability methods. *Struct. Saf.* **1992**, *11*, 95–107. [CrossRef]
17. Chen, J.S.; Yuan, J.X.; Ni, J. Compensation of non-rigid body kinematic effect on a machining center. *Trans. NAMRI* **1992**, *20*, 325–329.
18. Kiridena, V.; Ferreira, P. Kinematic modeling of quasistatic errors of three-axis machining centers. *Int. J. Mach. Tools Manuf.* **1994**, *34*, 85–100. [CrossRef]
19. Su, J.B. Research on Interval Analysis Method for Uncertainty in Engineering Structures and Its Application. Ph.D. Thesis, Hohai University, Nanjing, China, 2006.
20. Ye, P.Q.; Zhai, D.; Zhao, T.; Zhang, H. Sensitivity analysis of horizontal machining center space error to manufacturing error. *J. Tsinghua Univ. Nat. Sci. Ed.* **2011**, *51*, 587–591.
21. Guo, S.; Zhang, D.; Xi, Y. Global Quantitative Sensitivity Analysis and Compensation of Geometric Errors of CNC Machine Tool. *Math. Probl. Eng.* **2016**, *2016*, 2834718. [CrossRef]

22. Xi, F.; Verner, M.; Mechefske, C. Error sensitivity analysis for optimal calibration of parallel kinematic machines. In Proceedings of the ASME 2002 International Design Engineering Technical Conferences and Computers and Information in Engineering Conference, Portland, OR, USA, 29 September–2 October 2002; pp. 745–752.
23. Li, D.X.; Feng, P.F.; Zhang, J.F.; Yu, D.W. An identification method for key geometric errors of machine tool based on matrix differential and experimental test. *Proc. Inst. Mech. Eng. Part C J. Mech. Eng. Sci.* **2014**, *228*, 3141–3155. [CrossRef]
24. Cheng, Q.; Zhao, H.; Zhang, G.; Gu, P.; Cai, L. An analytical approach for crucial geometric errors identification of multi-axis machine tool based on global sensitivity analysis. *Int. J. Adv. Manuf. Technol.* **2014**, *75*, 107–121. [CrossRef]
25. Chen, G.; Liang, Y.; Sun, Y.; Chen, W.; Wang, B. Volumetric error modeling and sensitivity analysis for designing a five-axis ultra-precision machine tool. *Int. J. Adv. Manuf. Technol.* **2013**, *68*, 2525–2534. [CrossRef]
26. Zhang, S.; Xu, J. Transmission system accuracy optimum allocation for multiaxis machine tools' scheme design. *Proc. Inst. Mech. Eng. Part C J. Mech. Eng. Sci.* **2013**, *227*, 2762–2779.
27. Wu, W.; Rao, S.S. Uncertainty analysis and allocation of joint tolerances in robot manipulators based on interval analysis. *Reliab. Eng. Syst. Saf.* **2007**, *92*, 54–64. [CrossRef]
28. Geetha, K.; Ravindran, D.; Kumar, M.S.; Islam, M.N. Multi-objective optimization for optimum tolerance synthesis with process and machine selection using a genetic algorithm. *Int. J. Adv. Manuf. Technol.* **2013**, *67*, 2439–2457. [CrossRef]